Cement and Concrete Research 40 (2010) 956–965

Contents lists available at ScienceDirect

Cement and Concrete Research

journal homepage: http://ees.elsevier.com/CEMCON/default.asp

Cohesive fracture model for functionally graded fiber reinforced concrete

Kyoungsoo Park *, Glaucio H. Paulino, Jeffery Roesler

Department of Civil & Environmental Engineering, University of Illinois at Urbana-Champaign, 205 North Mathews Ave., Urbana, IL 61801, USA

ARTICLE INFO

Article history:
Received 14 October 2009
Accepted 2 February 2010

Keywords:
Concrete (E)
Fiber reinforced concrete (FRC) (E)
Constitutive relationship (C)
Cohesive fracture (C)
Fracture energy (C)

ABSTRACT

A simple, effective, and practical constitutive model for cohesive fracture of fiber reinforced concrete is proposed by differentiating the aggregate bridging zone and the fiber bridging zone. The aggregate bridging zone is related to the total fracture energy of plain concrete, while the fiber bridging zone is associated with the difference between the total fracture energy of fiber reinforced concrete and the total fracture energy of plain concrete. The cohesive fracture model is defined by experimental fracture parameters, which are obtained through three-point bending and split tensile tests. As expected, the model describes fracture behavior of plain concrete beams. In addition, it predicts the fracture behavior of either fiber reinforced concrete beams or a combination of plain and fiber reinforced concrete functionally layered in a single beam specimen. The validated model is also applied to investigate continuously, functionally graded fiber reinforced concrete composites.

1. Introduction

Fiber reinforced concrete (FRC) composites have been utilized to improve the performance of plain concrete materials and to repair and retrofit structures [1–8]. Fibers can be spatially (or functionally) distributed to improve structural performance while minimizing the amount of fibers. These spatially varied microstructures created by nonuniform distributions of reinforcement phase are called functionally graded materials (FGMs) [9]. Recently, functionally graded fiber-reinforced cement composite have been developed by using the extrusion technique [10] and the Hatschek process [11] in order to improve the structural performance of a component while reducing its material cost.

In order to explicitly consider the larger fracture process zone in cementitious materials, Hillerborg et al. [12] expanded the cohesive zone model concept [13,14] to concrete by combining fracture mechanics and the finite element method. The major challenge in the cohesive zone model is the determination of the traction–separation relationship, which represents the nonlinear fracture process zone of a material. For plain concrete, a linear softening model was employed by Hillerborg et al. [12], and a bilinear softening model was introduced by Petersson et al. [15]. Since then, a bilinear softening model has been widely utilized to investigate plain concrete fracture behavior [16].

The nonlinear fracture process zone of FRC has been specifically investigated by various methods such as (a) direct tension tests [17–19], (b) fiber pull-out tests [20–24], (c) indirect methods [25,26], and (d) inverse analysis [27,28]. *Direct tension tests* are performed to estimate fracture parameters and the tensile versus crack separation relationships [17–19]. However, because of material nonhomogeneity, the uniaxial tension test results in spontaneous multiple crack growth. Therefore, a specimen tends to asymmetric modes of failure unless the experimental setup is extremely well prepared [29]. Fracture parameters can be also calibrated by utilizing *fiber pull-out tests*. For example, Li et al. [21,22] developed a micromechanics-based model by integrating individual fiber contributions. Since the model is based on 11 parameters (4 concrete parameters, 4 fiber parameters, and 3 interface parameters), a more simplified model is desirable for civil engineering applications [30]. Cohesive interactions for FRC can also be indirectly estimated from the experimental load–displacement curve, i.e. *indirect method*. For instance, Guo et al. [25] approximated a FRC softening model as a bilinear softening model from the concrete's tensile strength, fracture energy, and the known tail of a three-point bending load–displacement curve. An *inverse analysis* can also be employed to calibrate the softening model such that the best predicted load–displacement curve is achieved. Sousa and Gettu [27], and Slowik et al. [28] determined a piecewise linear cohesive model of FRC by minimizing the difference between simulation results and experimental test results.

Based on the traction–separation relationship, crack propagation phenomena in FRC materials have been investigated by employing several analytical or numerical methods such as a semi-analytical model [31], a stress intensity factor (LEFM) approach [30], a series of nonlinear springs [26], and an irregular lattice model [32]. Furthermore, finite element-based cohesive zone models [33–35], which is the choice of numerical methods in this paper, have been utilized for a wide range of materials such as plain concrete [29,36], reinforced concrete [33], asphalt concrete [37], and functionally graded materials

* Corresponding author. Tel.: +1 217 265 8042, +1 217 265 0218; fax: +1 217 265 8040.
E-mail address: kpark16@illinois.edu (K. Park).

0008-8846/$ – see front matter © 2010 Elsevier Ltd. All rights reserved.
doi:10.1016/j.cemconres.2010.02.004

Table 1
Concrete mixture proportions (kg/m^3).

Plain concrete	Water	Type I cement	Coarse aggregate	Fine aggregate
	183	360	976	807

(1 kg/m^3 = 1.687 lb/yd^3).

Table 2
Average fracture parameters for plain concrete and FRC.

	f'_t (MPa)	G_f (N/m)	G_F or G_{FRC} (N/m)	$CTOD_c$ (mm)
Plain concrete	3.44	38.3	120	0.016
FRC	4.22	37.1	3531	0.016

(1 MPa = 0.145 ksi and 1 N/m = 0.06852 lb/ft and 1 mm = 0.03937 in.).

[8,38] in order to evaluate nonlinear traction–separation relationships. Alternatively, the generalized/extended finite element method has been employed to simulate cohesive cracks for quasi-brittle materials [39–42].

A simple constitutive model for FRC fracture is proposed in this paper on the basis of measured fracture parameters, which are estimated by three-point bending and split tensile tests. The proposed FRC model is defined as trilinear softening for use with concrete containing synthetic fibers without strain hardening. The model is validated by predicting the fracture behavior of functionally layered FRC beams. Furthermore, the effects of alternative fiber spatial distributions are investigated with the validated computational model. This type of computation for functionally graded (or layered) FRC can potentially be utilized in designing more economical structural systems, for example, in airport and highway pavements, commercial and precast slabs, structural elements, etc.

2. Experimental observations

In order to investigate fracture mechanisms of FRC, the experiments performed by Roesler et al. [43] are utilized. The plain concrete mixture proportions are given in Table 1 while the FRC has the same proportions except for the incorporation of synthetic fiber at a dosage of 0.78% by volume (7.2 kg/m^3 or 12.1 lb/yd^3). Fiber length is 40 mm (1.6 in.) with rectangular cross section (1.5 × 0.105 mm or 0.0551 × 0.00413 in.) and aspect ratio of 90. Fracture parameters are determined from the split cylinder and a three-point bending test, as shown in Table 2. The tensile strength, the initial fracture energy (G_f), and the critical crack tip opening displacement ($CTOD_c$) of plain concrete are similar to those of FRC. Because G_f and $CTOD_c$ are associated with peak load capacities for those specimen geometries, the inclusion of fibers does not significantly influence the peak load behavior of three-point bending tests. However, the total fracture energy of plain concrete is 120 N/m (7.9 lb/ft) while the total fracture energy of FRC is 3531 N/m (232 lb/ft). Most of the external energy is dissipated at relatively large crack opening widths for FRC.

The experimental test program has four different layered concrete material combinations placed in a three-point bending specimen. Fig. 1 demonstrates the four composite beams: full depth of plain concrete, full depth of FRC, FRC layer at the bottom, and FRC layer at the top, while Fig. 2 illustrates the geometry of the beams. The composite beams were subjected to 10 cycles of loading and unloading, followed by a final load cycle until complete specimen failure. The envelope curve is then obtained by circumscribing the loading/unloading cycles for each test. The average load versus crack mouth opening displacement (CMOD) envelope curves for each beam combination is plotted in Fig. 3. An example, seen in Fig. 4, demonstrates two experimental beam data with FRC layer at the top together with the average load–CMOD curve. A close-up of the load–CMOD curves in Fig. 3 illustrates that the elastic, peak load, and early post-peak load behaviors are similar for each beam combination when the CMOD is smaller than 0.2 mm (0.079 in.). However, at relatively larger crack opening widths (e.g., CMOD = 1 mm or 0.039 in.), the plain concrete specimens demonstrate complete failure while the FRC layered specimens are able to sustain a certain level of load because of the fiber bridging zone. Similarly, other researchers have reported that polypropylene fibers do not have significant effects on the peak load and early post-peak load behavior, but provide extra load carrying capacity at relatively larger crack opening widths [44,45]. As a result of this distinct behavior, the fracture process zone (or cohesive crack model) can be sub-divided into the aggregate bridging zone and the fiber bridging zone.

3. Constitutive relationship of cohesive zone models

In this section, a bilinear softening model for plain concrete is presented. The traction–separation relationship for FRC is proposed which considers the fracture mechanisms of both plain concrete and FRC. Afterwards, a constitutive model for functionally graded FRC is proposed.

3.1. Bilinear softening model for plain concrete

Progressive fracture mechanisms of plain concrete can be idealized as a distributed micro-crack zone, a bridging zone, and a traction free

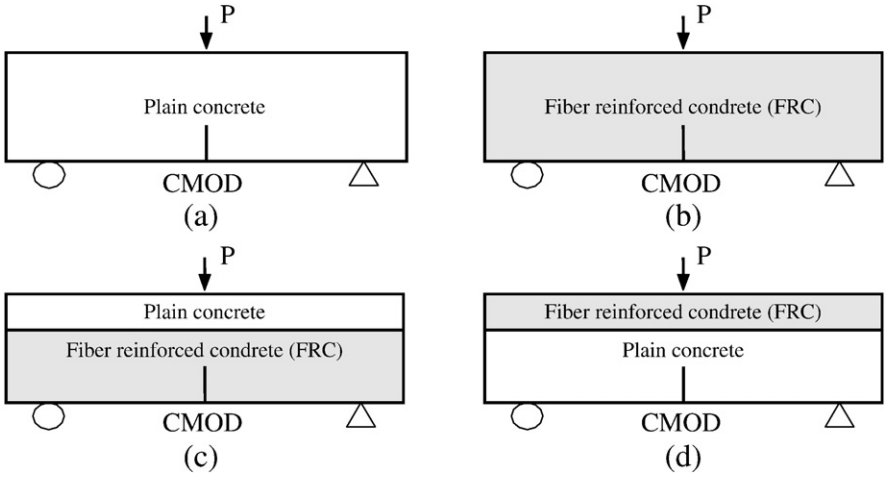

Fig. 1. Four different combinations of FRC layers: (a) full depth of plain concrete; (b) full depth of FRC; (c) FRC layer at the bottom; (d) FRC layer at the top.

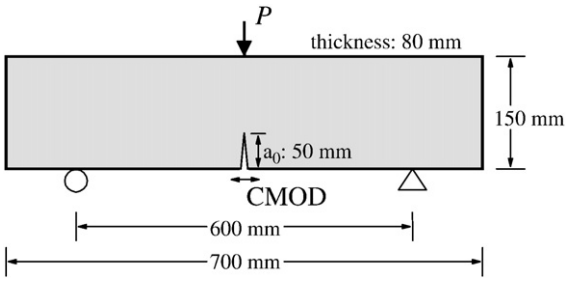

Fig. 2. Geometry of three-point bending specimens.

macro-crack zone [46], as shown in Fig. 5. Micro-cracks exist in the concrete ahead of the bridging zone. As the stress approaches the cohesive strength (e.g., material's tensile strength, f_t'), micro-cracks extend and coalesce, which produce the bridging zone, also called the nonlinear fracture process zone. This zone results from crack branching and interlocking typically as a result of the weak interface between the aggregates and cement matrix. The process zone is approximated with the concept of the cohesive zone model, which leads to the relationship between traction and separation. When a crack opening width is greater than a certain value, called the final crack opening width (w_f), a macroscopic crack appears which subsequently cannot transfer traction along its surfaces.

In order to approximate the nonlinear fracture process zone of plain concrete, this paper utilizes a bilinear softening model (see Fig. 5), which provides a systematic determination of the softening model [47]. The bilinear softening model is defined by four experimental fracture parameters:

- tensile strength (f_t')
- initial fracture energy (G_f)
- total fracture energy (G_F) and
- critical crack tip opening displacement ($CTOD_c$).

The total fracture energy is calculated by the work-of-fracture method [48] with the consideration of the specimen's self-weight. The initial fracture energy and $CTOD_c$ are estimated by either the size effect method [49,50] or the two-parameter fracture model [51]. The size effect method and the two-parameter fracture model are based on the concept of the equivalent elastic crack model, which defines the critical crack length at the peak load. The calculated effective crack length, for example, leads to the estimation of $CTOD_c$ and the critical stress intensity factor (K_{IC}). The initial fracture energy is obtained by $G_f = K_{IC}^2/E$, where E is elastic modulus. Thus, the fracture parameters, G_F, G_f and $CTOD_c$, are estimated by a single fracture test, i.e. three-point bending test. Although the split tensile strength does not represent the true tensile strength of the concrete, it can be used to indirectly infer the tensile strength of the material, recognizing the influence of specimen geometry and the width of the load-bearing strip [52].

The initial fracture energy and tensile strength define the horizontal axis intercept (w_1) of the initial softening slope, expressed as:

$$w_1 = 2G_f / f_t'. \tag{1}$$

The crack opening width (w_k) at the kink point has been hypothesized [47] as:

$$w_k = CTOD_c, \tag{2}$$

which results in the determination of the stress ratio (ψ) at the kink point, i.e.

$$\psi = 1 - \frac{CTOD_c f_t'}{2G_f}. \tag{3}$$

The final crack opening width is calculated as:

$$w_f = \frac{2}{\psi f_t'}[G_F - (1-\psi)G_f], \tag{4}$$

which is obtained by equating the total fracture energy with the area under the bilinear softening model for plain concrete.

3.2. Trilinear softening model for FRC

The fracture mechanisms of FRC are different from those of plain concrete due to the inclusion of discrete fibers. Although fibers at low volume fractions do not generally influence the tensile strength or early post-peak behavior, the inclusion of fibers does increase the fracture process zone size [46]. The nonlinear fracture process zone of FRC

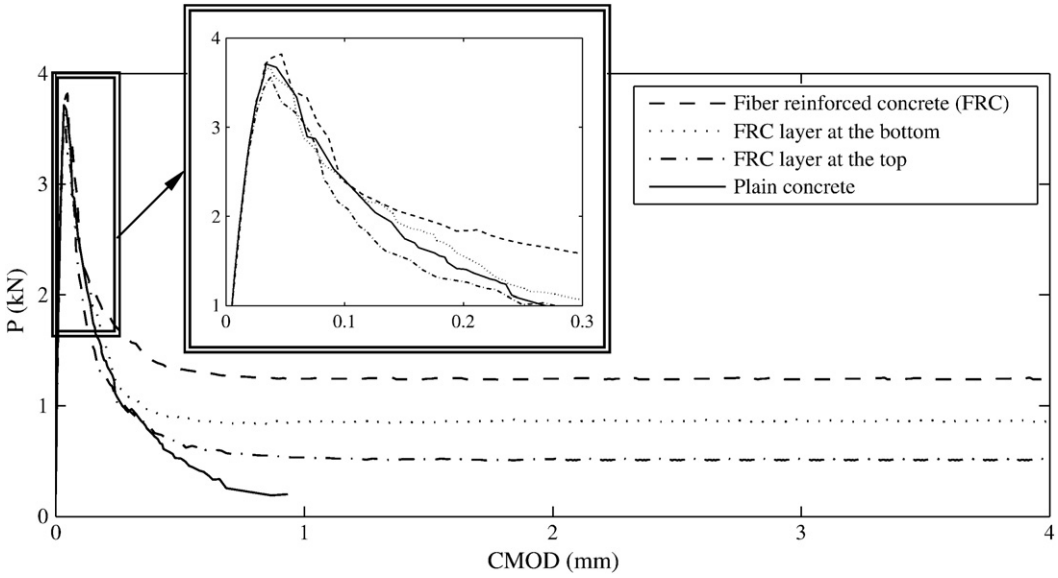

Fig. 3. Average load–CMOD envelope curves for three-point bending specimens with the four combinations of concrete layers.

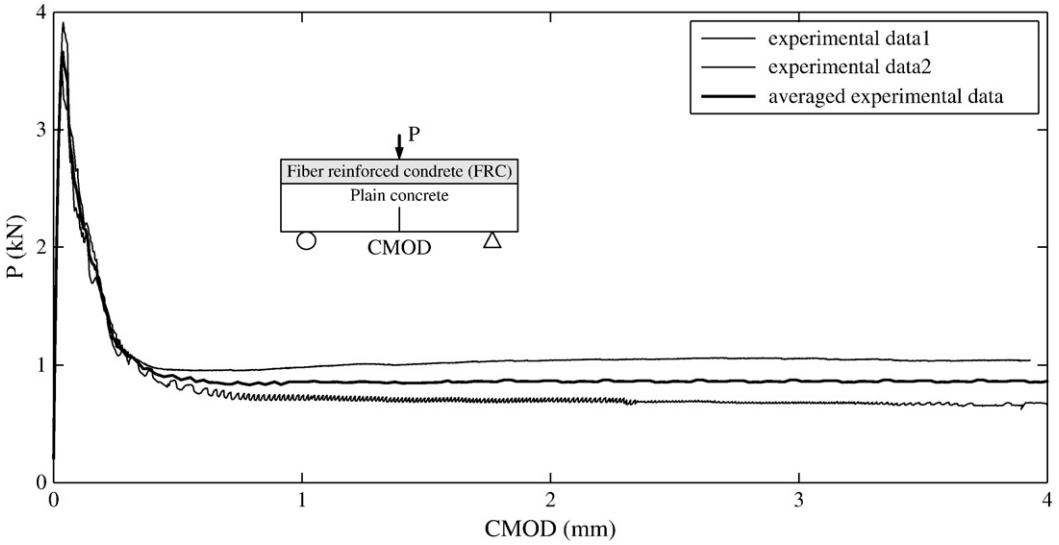

Fig. 4. Load–CMOD envelope curves of two experimental data and averaged experimental data for FRC layer at the top.

includes micro-cracking, aggregate interlocking, fiber de-bonding, and fiber pull-out [46,53]. Plain concrete fracture mechanisms generally dominate at small crack opening widths. Conversely, mechanisms associated with fibers contribute a significant role at relatively wider crack opening widths. Experimental observations have also demonstrated a distinction between the aggregate and fiber bridging zones. As a result, the nonlinear fracture process zone for FRC is further divided into the aggregate bridging zone and the fiber bridging zone, as shown in Fig. 6.

The aggregate bridging zone is approximated by the same softening model as the plain concrete. The fiber bridging zone is assumed to represent the concrete material damage at wider crack opening width and is approximated by a linear descending slope with respect to the increase in the crack opening width as seen in Fig. 6. The linear descending slope is associated with the energy balance concept [54,55]: a crack will propagate when the energy available to extend a unit area of crack is equal to the energy required. With the inclusion of fibers to plain concrete, the additional energy is required to de-bond and pull-out the fibers from the concrete matrix, not necessarily to create additional fractured surfaces. The additional energy corresponds to the difference between the total fracture energy of plain concrete and the total fracture energy of FRC, which is the shaded region in the proposed softening model (see Fig. 6). The proposed representation of the fiber bridging zone may not be the best choice for certain fiber types and high volume fractions that result in a secondary peak in the global load–CMOD response curve. Significant distributed micro-cracking can lead to strain hardening behavior in the post cracking stage [10,30], and inverse analysis techniques of strain hardening load–deflection curves for FRC [27,28] have resulted in different traction–separation relationship curves than that shown in Fig. 6.

The proposed FRC softening model is determined by six experimental fracture parameters:

- tensile strength (f'_t),
- initial fracture energy (G_f),
- total fracture energy of plain concrete (G_F),
- critical crack opening displacement ($CTOD_c$),
- total fracture energy of FRC (G_{FRC}) and
- fiber length (L_f).

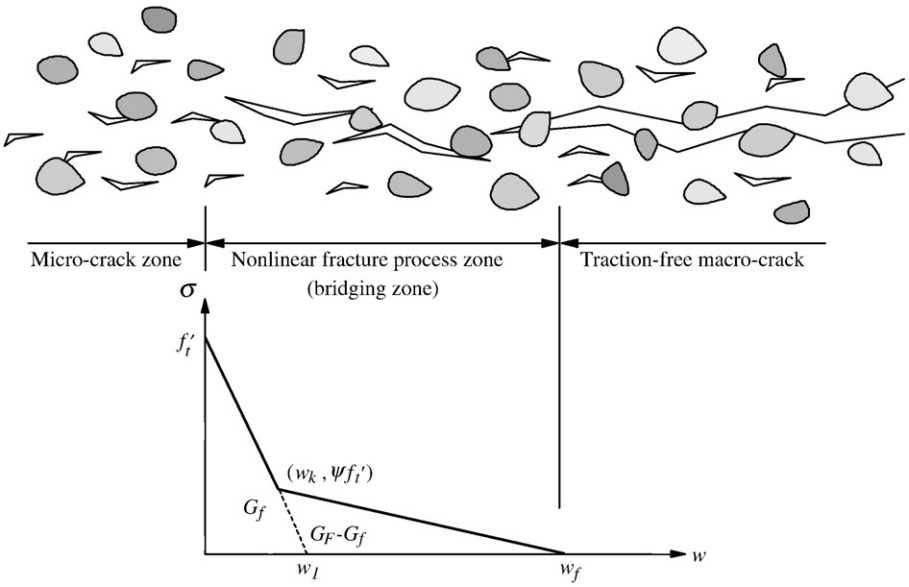

Fig. 5. Plain concrete fracture mechanisms and experimental fracture parameter based softening model.

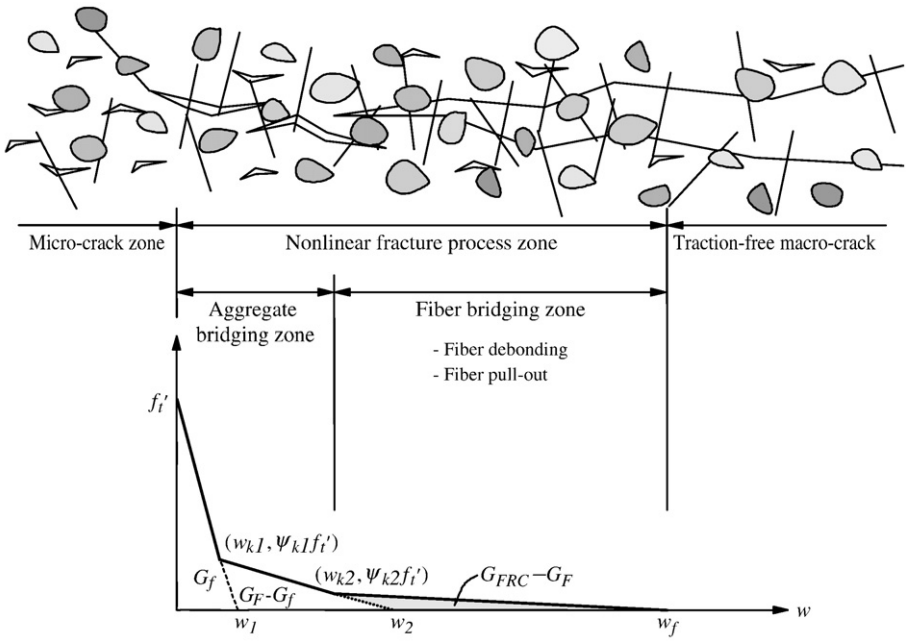

Fig. 6. Fracture mechanisms and the experimental fracture parameter based softening model for fiber reinforced concrete (FRC).

The first four parameters define the bilinear softening of the plain concrete, as discussed previously. The first kink point (w_{k1},$\psi_1 f_t'$) in the FRC softening model (Fig. 6) is the same as the kink point (w_k, $\psi f_t'$) in the plain concrete softening model (Fig. 5), which is calculated by Eqs. (2) and (3). The total fracture energy of FRC, which corresponds to the area under the trilinear softening model, is estimated by the work-of-fracture method [48] with the full load–deflection curves. The CMOD at the onset of specimen failure is approximately 45 mm. Notice that the total fracture energy of FRC is not the same as "toughness — the energy equivalent to the area under the load–deflection curve up to a specified deflection" defined in ASTM standard C1018 [56] or C1609 [57]. The horizontal axis intercept (w_2) of the second softening slope (Fig. 6) is the same as the final crack opening width (Eq. (4)) in the plain concrete softening model (Fig. 5). Next, the final crack opening width (w_f) can be estimated as a quarter to one-half of the fiber length ($L_f/4$, $L_f/2$), which corresponds to the average pull-out length for randomly distributed fibers reported in the literature [58–60]. Finally, the second kink point position (w_{k2}, $\psi_2 f_t'$) is calculated from the additional fracture energy ($G_{FRC} - G_F$) due to the inclusion of fibers and is expressed as the following,

$$\psi_2 = \frac{2(G_{FRC} - G_F)}{f_t'(w_f - w_2)}, \tag{5}$$

and

$$w_{k2} = w_2 - \frac{\psi_2}{\psi_1}(w_2 - w_{k1}). \tag{6}$$

3.3. Functionally graded FRC

Fiber volume fraction can be spatially varied, i.e., functionally graded FRC, in order to achieve similar structural performance in an engineered system at a lower cost. The effect of functionally layered FRC with regards to fracture energy and residual load capacity is investigated by means of computational simulation with the cohesive zone model [8], which can subsequently be applied to concrete slabs, pavements, or structural elements.

The constitutive model for functionally graded FRC is extended from the model of homogeneous FRC, i.e. trilinear softening model. The fracture parameters associated with the fiber bridging zone in the trilinear softening model are the total fracture energy (G_{FRC}) and fiber length (L_f). If fiber length is uniform in functionally graded FRC, G_{FRC} is the only fracture parameter that spatially varies with respect to fiber volume fraction. The functional form $G_{FRC}(x)$ is computed by interpolating the total fracture energy at the nodal locations. The spatial variation of G_{FRC} also leads to a change in the second kink point in the trilinear softening model. The change of the fracture parameters in the constitutive model is managed by utilizing the generalized

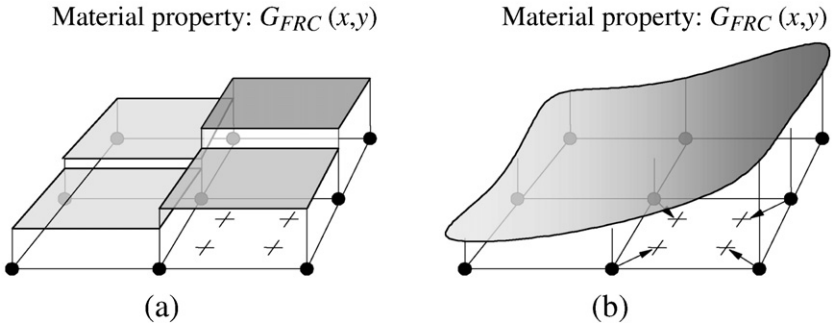

Fig. 7. Spatial variation of a material property for (a) homogeneous elements; and (b) graded elements.

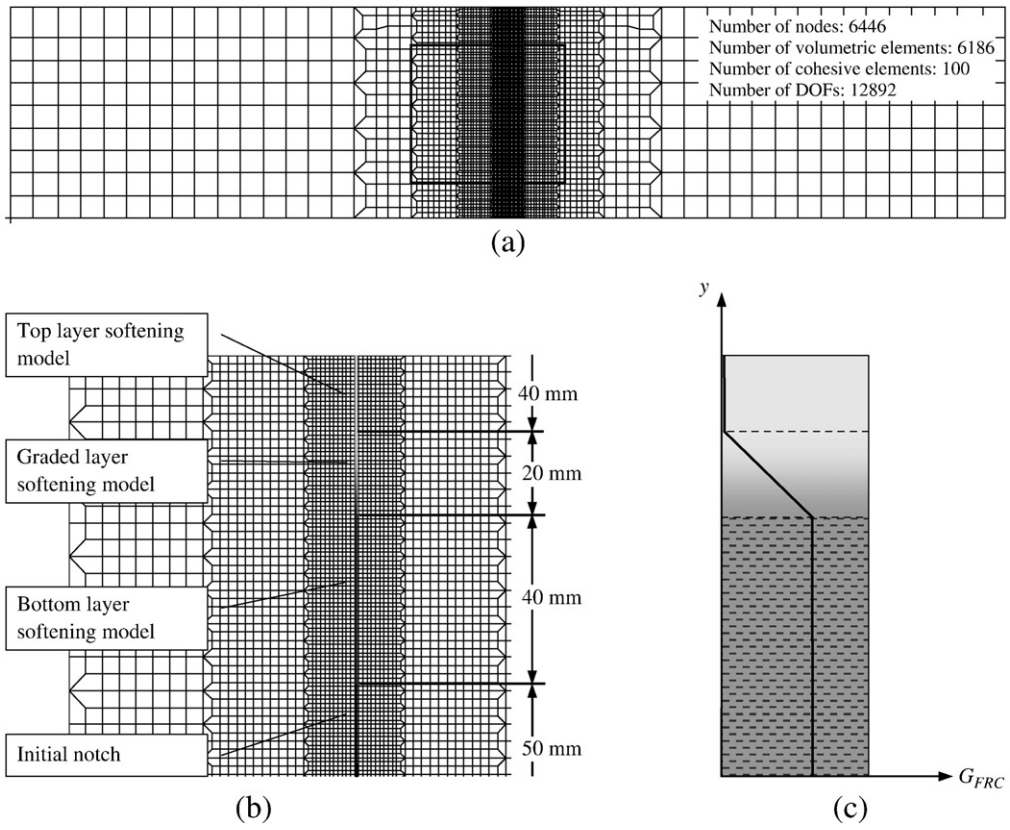

Fig. 8. (a) Typical mesh for the finite element analysis; (b) zoom in of the mesh along the cohesive fracture region; (c) example of the total fracture energy variation.

isoparametric formulation (GIF) [61,62], which is explained in the next section.

4. Computational simulation

The trilinear FRC softening model is validated by predicting the load versus CMOD curves of experimental FRC beams in conjunction with a finite element-based cohesive zone model. Cohesive surface elements are developed as a user-defined element (UEL) subroutine in the commercial software ABAQUS. Computer simulations of functionally graded fiber reinforced concrete are also analyzed and presented for three different fiber distributions.

When a material property varies spatially, the constitutive relationship is also a function of location. In traditional finite element formulation, the constitutive law is independent of position within an element (i.e. homogeneous element). Kim and Paulino [62] proposed the generalized isoparametric formulation (GIF) to represent material gradation within an element (i.e. graded element). In the isoparametric formulation, displacement fields (u) and geometric coordinates (x) are interpolated from nodal quantities (u_i, x_i) using

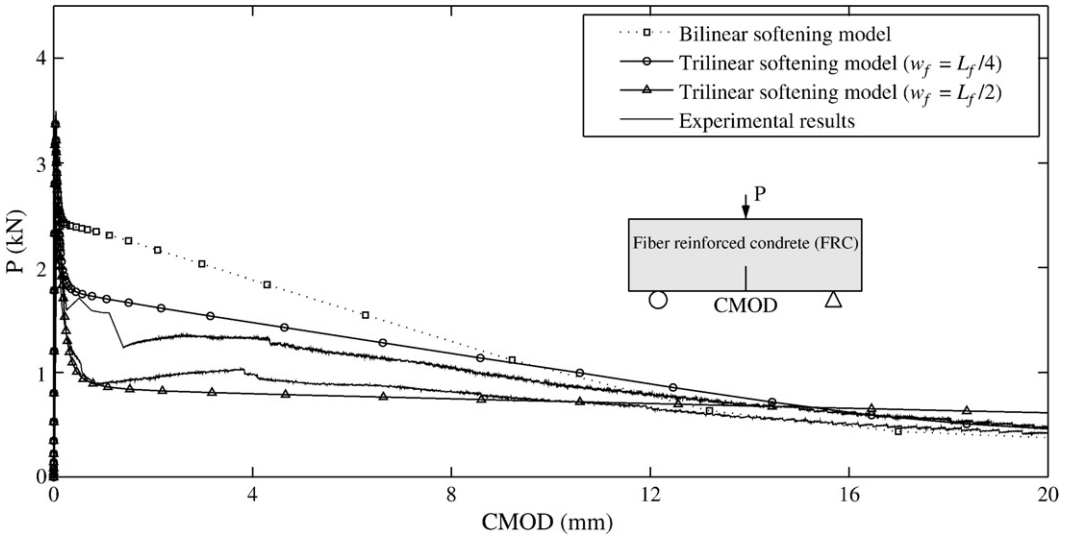

Fig. 9. Comparison between experimental results and simulation results for full depth FRC specimens.

the same shape functions (N_i). Similarly, in the GIF, material properties (e.g. fracture energy of FRC, G_{FRC}) at Gaussian integration points are also interpolated from nodal points (G_{FRCi}) using the same shape functions,

$$G_{FRC} = \sum_{i=1}^{nel} N_i G_{FRCi}, \tag{7}$$

where *nel* is the number of nodes in an element. Fig. 7(a) and (b) demonstrates spatial variations of material properties for homogeneous and graded elements, respectively. Homogeneous elements generally result in stress jumps due to the discontinuity of material properties while graded elements reduce these effects. Moreover, graded finite elements typically provide more accurate local stress than conventional homogeneous elements [62,63], and thus a coarser mesh can be used in the material gradation region, decreasing computational costs.

The functionally layered FRC composite beams and the corresponding specimen geometry employed in this research are described in Figs. 1 and 2, respectively. The elastic modulus of plain concrete was 27.2 GPa (3950 ksi), and the modulus of FRC was 26.5 GPa (3850 ksi). Additional fracture parameters are listed in Table 2. In the computational simulation, the bilinear softening component, i.e. the aggregate bridging zone, is determined by the fracture parameters of plain concrete while the linear descending part in the FRC softening model, i.e., the fiber bridging zone, is estimated by the fracture parameters of FRC.

In the finite element analysis, general volumetric elements represent the elastic behavior of the concrete materials while cohesive surface elements characterize the fracture behavior of the concrete materials. The mesh for the finite element analysis is given in Fig. 8(a), and a zoom in of the mesh along the cohesive fracture region is shown in Fig. 8(b). The finite element mesh consists of 6444 nodes, 6186 volumetric elements, and 100 cohesive surface elements. The cohesive elements are inserted along potential crack paths, and an initial ascending slope is introduced in the constitutive relationship of the cohesive zone model, i.e., intrinsic cohesive zone modeling [37,47]. Since mode I fracture is only considered in this study, the cohesive elements are inserted along the vertical load line. The size of the cohesive element was selected to be 1 mm, which is small enough

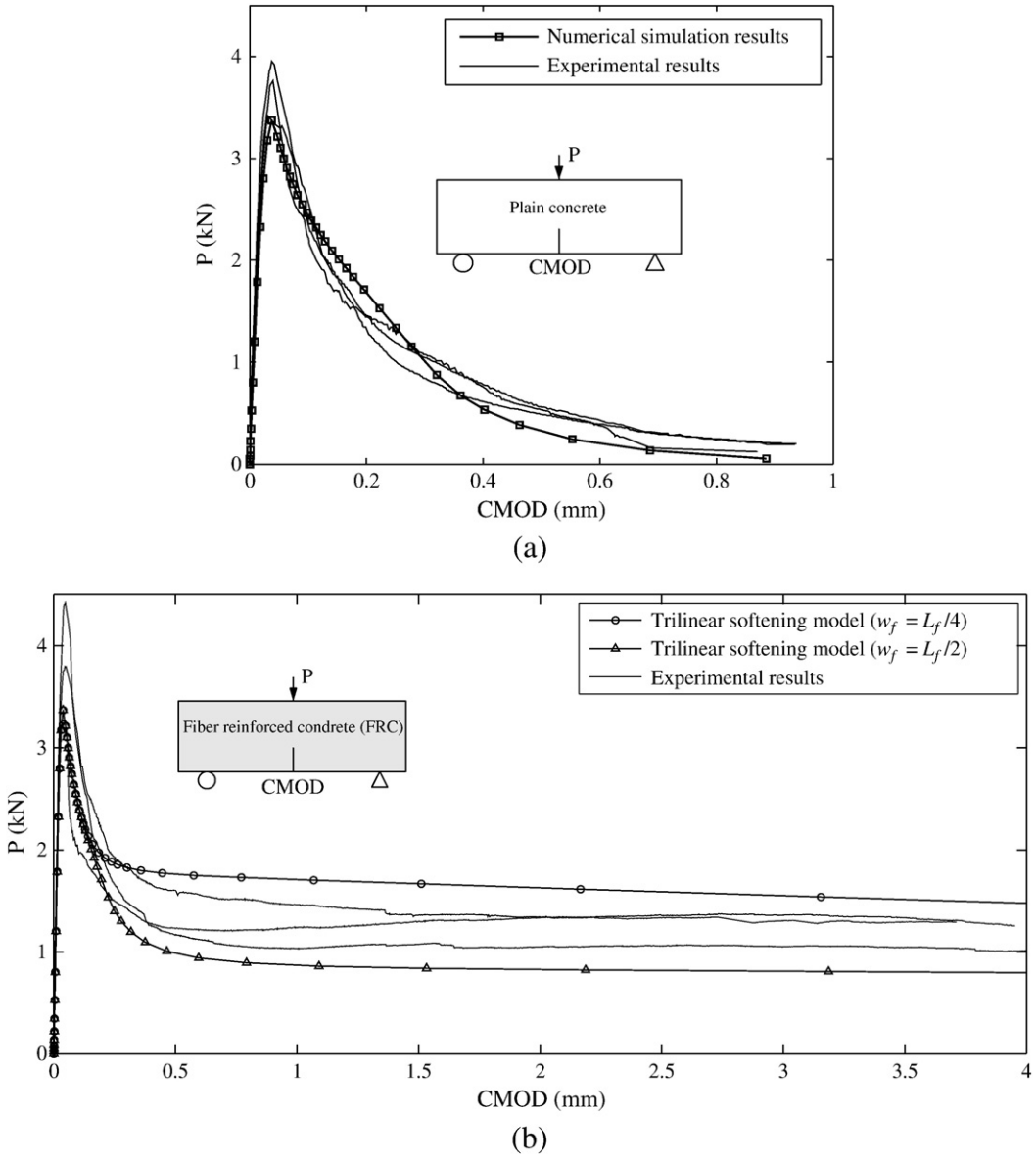

Fig. 10. Comparison between experimental and simulation results with respect to the different combination of FRC layers: (a) full depth plain concrete; (b) full depth FRC; (c) FRC layer at the bottom; (d) FRC layer at the top.

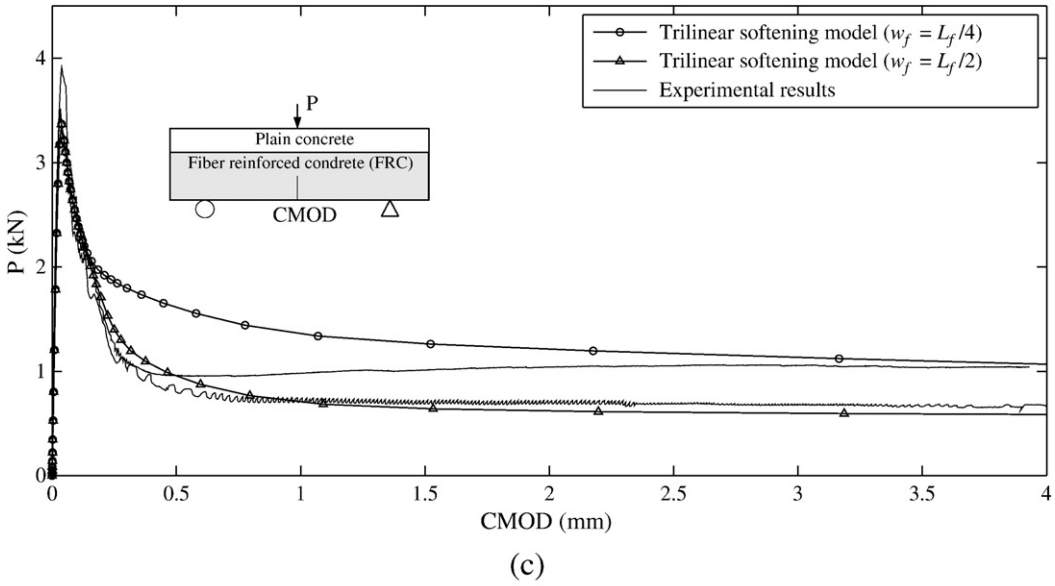

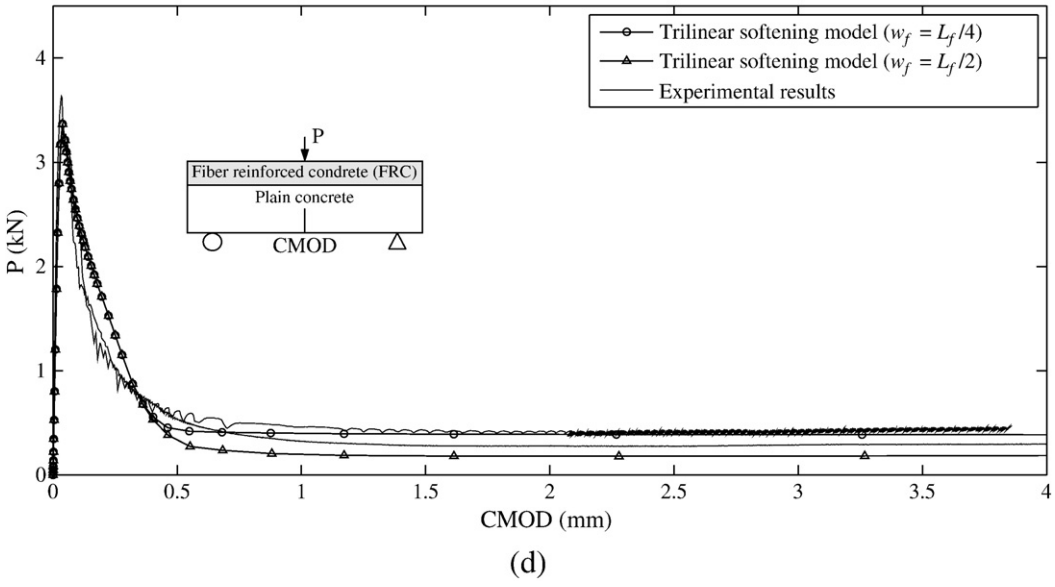

Fig. 10 (*continued*).

to capture the local fracture process in this problem [36]. Between the top and the bottom layers, the graded region is introduced by using the GIF in order to reduce stress discontinuity, and to represent concrete mixture blending between the top and bottom layers in the casting process. In the computational simulation of functionally layered concrete, the total fracture energy of FRC (G_{FRC}) is assumed to vary linearly between the two layers as an initial estimate, as shown in Fig. 8(c) for plain (top layer) and FRC (bottom layer).

5. Results and discussion

Results from the finite element simulations with the cohesive zone model are compared with the experimental load–CMOD curves for the four different combinations of FRC layers shown in Fig. 1. The first simulation shown in Fig. 9 demonstrates the fracture behavior of full depth FRC specimens. In the trilinear (FRC) softening model, the final crack opening width of $L_f/2$ and $L_f/4$ (half and quarter of the fiber

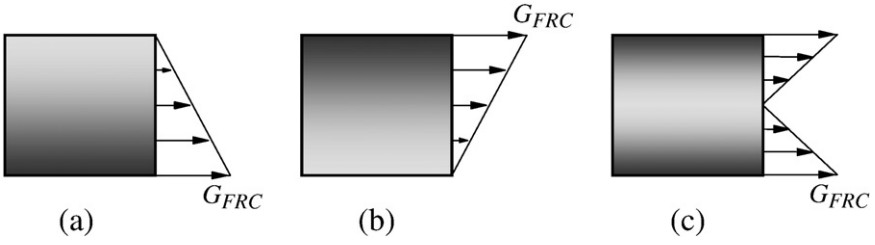

Fig. 11. Spatial variation of fiber volume fraction from the initial notch to the top of a specimen.

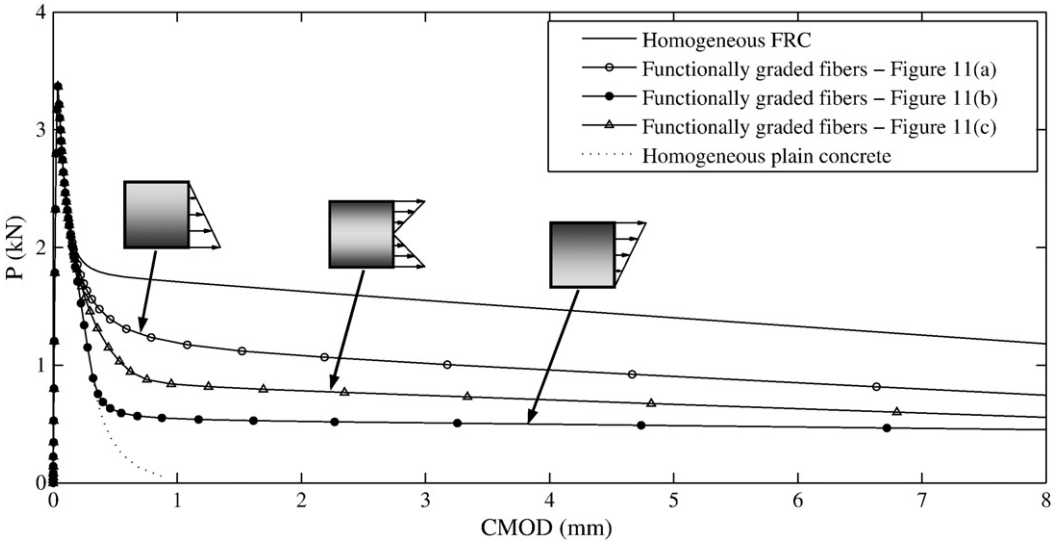

Fig. 12. Simulations of homogeneous and functionally graded fiber reinforced concrete specimens.

length, respectively) are utilized. The simulation result with the bilinear softening model is also illustrated in Fig. 9 for comparison purpose. The bilinear softening model significantly overestimates the experimental load–CMOD curves except at very large opening widths, while the proposed FRC softening model correctly bounds the overall load–CMOD curves. Fig. 10 presents the simulation results with respect to the four different combinations of FRC layers. Simulation results demonstrate the global response agreement between the experiments and the model in the elastic, peak, and post-peak regions. The difference between the peak load of computational result and the average peak load of experimental data is between 3 and 11%. The model cannot locally capture the slight increase in residual load, shown in Fig. 10(b) and (c) because the constitutive model does not consider the individual fiber pull-out effect. In the plateau region, the $w_f = L_f/2$ illustrates the lower bound of the load–CMOD curves while the $w_f = L_f/4$ demonstrates the upper bound of the load–CMOD curves in this study.

The effects of fiber gradation are also investigated with the validated computational tool. Fig. 11 illustrates potential spatial distribution of the total fracture energy of FRC for several functionally graded FRC composite beams. The functionally graded FRC beams are compared with homogeneous beams of plain concrete and FRC, shown in Fig. 12. All specimens respond with the same elastic, peak load, and early post-peak load behaviors, but demonstrate markedly different load carrying capacities when the CMOD is greater than 0.5 mm (0.02 in). The load carrying capacities in the plateau region depend on the fiber distributions. If one assumes that the total fracture energy of FRC is proportional to a fiber volume fraction, the functionally graded FRC specimens contain half of the fiber volume fraction as the homogeneous FRC specimens. The fiber distribution in Fig. 11(a) provides more than half of the load carrying capacity in the post-peak region relative to the homogeneous FRC specimen. However, the fiber distribution of Fig. 11(b) provides less than half of the post-peak load carrying capacity with respect to the homogeneous FRC case. The fiber distribution of Fig. 11(c) does not provide as much load carrying capacity as that of Fig. 11(a) either. However, this bilinear fiber gradation (Fig. 11(c)) provides the same effective resistances for both top-down cracking and bottom-up cracking that may occur simultaneously in slab-on-ground applications with certain loading configurations. As a result, functionally graded FRC has potential to maximize the load carrying capacity of structures with lower effective volumes of fibers relative to full depth FRC structures.

6. Conclusion

A simple and practical trilinear softening model for fiber reinforced concrete (FRC) is proposed, which is defined by the following estimated experimental fracture parameters: the tensile strength (f'_t), initial fracture energy (G_f), total fracture energy of plain concrete (G_F), critical crack opening displacement ($CTOD_c$), fiber length (L_f), and total fracture energy of FRC (G_{FRC}). The model separates fracture mechanisms of FRC into the aggregate bridging zone and the fiber bridging zone. The aggregate bridging zone is related to the total fracture energy of plain concrete (G_F) while the fiber bridging zone is associated with the difference between the total fracture energy of FRC and the total fracture energy of plain concrete ($G_{FRC} - G_F$). The proposed FRC softening model is able to predict the load–CMOD curves for different combinations of FRC and plain concrete layers. Furthermore, the effects of fiber spatial distributions are investigated by introducing a specially graded cohesive element into the computational simulations. The simulation results illustrate that functionally graded (or layered) FRC can potentially be used to design more economical structural systems. Functionally graded (or layered) FRC is one application of multifunctional and functionally graded concrete materials for the civil infrastructure. Varying concrete constituents (e.g. fibers, aggregate type, or air voids) can provide extra flexibility in designing efficient structural systems.

Acknowledgments

The authors would like to acknowledge support from the National Science Foundation (NSF) through grant CMMI #0800805. We also acknowledge support through the Center of Excellence for Airport Technology (CEAT) provided by the O'Hare Modernization Program (OMP) and the City of Chicago for their financial support in this study. The information presented in this paper is the sole opinion of the authors and does not necessarily reflect the views of the sponsoring agencies.

References

[1] J.P. Romualdi, G.B. Batson, Mechanics of crack arrest in concrete, American Society of Civil Engineers Proceedings, Journal of the Engineering Mechanics Division 89 (EM3) (1963) 147–168.
[2] M. Grzybowski, S.P. Shah, Shrinkage cracking of fiber reinforced concrete, ACI Materials Journal 87 (2) (1990) 138–148.

[3] P. Balaguru, A. Khajuria, Properties of polymeric fiber-reinforced concrete, Transportation Research Record 1532 (1996) 27–35.
[4] V.C. Li, H. Horii, P. Kabele, T. Kanda, Y.M. Lim, Repair and retrofit with engineered cementitious composites, Engineering Fracture Mechanics 65 (2) (2000) 317–334.
[5] F.J. Alaee, B.L. Karihaloo, Retrofitting of reinforced concrete beams with CARDIFRC, Journal of Composites for Construction 7 (3) (2003) 174–186.
[6] J.R. Roesler, S.A. Altoubat, D.A. Lange, K.-A. Rieder, G.R. Ulreich, Effect of synthetic fibers on structural behavior of concrete slabs-on-ground, ACI Materials Journal 103 (1) (2006) 3–10.
[7] N. Banthia, M. Sappakittipakorn, Toughness enhancement in steel fiber reinforced concrete through fiber hybridization, Cement and Concrete Research 37 (9) (2007) 1366–1372.
[8] F. Evangelista Jr., J.R. Roesler, G.H. Paulino, Numerical simulations of the fracture resistance of functionally graded concrete materials, Transportation Research Record 2113 (2009) 122–131.
[9] G.H. Paulino, Fracture of functionally graded materials, Engineering Fracture Mechanics 69 (14–16) (2002) 1519–1520.
[10] B. Shen, M. Hubler, G.H. Paulino, L.J. Struble, Functionally-graded fiber-reinforced cement composite: processing, microstructure, and properties, Cement & Concrete Composites 30 (8) (2008) 663–673.
[11] C.M.R. Dias, H. Savastano Jr and V.M. John, Exploring the potential of functionally graded materials concept for the development of fiber cement, Construction and Building Materials 24 (2), (2010) 140–146.
[12] A. Hillerborg, M. Modéer, P.E. Petersson, Analysis of crack formation and crack growth in concrete by means of fracture mechanics and finite elements, Cement and Concrete Research 6 (6) (1976) 773–781.
[13] G.I. Barenblatt, The formation of equilibrium cracks during brittle fracture: general ideas and hypotheses, axially symmetric cracks, Applied Mathematics and Mechanics 23 (1959) 622–636.
[14] D.S. Dugdale, Yielding of steel sheets containing slits, Journal of the Mechanics and Physics of Solids 8 (2) (1960) 100–104.
[15] P.E. Petersson, Crack Growth and Development of Fracture Zones in Plain Concrete and Similar Materials, Lund Institute of Technology, Sweden, 1981.
[16] Z.P. Bazant, J. Planas, Fracture and Size Effect in Concrete and other Quasibrittle Materials, CRC Press, Boca Raton, 1998.
[17] J.G.M. van Mier, M.R.A. van Vliet, Uniaxial tension test for the determination of fracture parameters of concrete: state of the art, Engineering Fracture Mechanics 69 (2) (2002) 235–247.
[18] V.S. Gopalaratnam, S.P. Shah, Softening response of plain concrete in direct tension, Journal of the American Concrete Institute 82 (3) (1985) 310–323.
[19] Y. Wang, V.C. Li, S. Backer, Experimental determination to tensile behavior of fiber reinforced concrete, ACI Materials Journal 87 (5) (1990) 461–468.
[20] H. Stang, S.P. Shah, Failure of fibre-reinforced composites by pull-out fracture, Journal of Materials Science 21 (3) (1986) 953–957.
[21] V.C. Li, W. Youjiang, S. Backer, A micromechanical model of tension-softening and bridging toughening of short random fiber reinforced brittle matrix composites, Journal of the Mechanics and Physics of Solids 39 (5) (1991) 607–625.
[22] V.C. Li, H. Stang, H. Krenchel, Micromechanics of crack bridging in fibre-reinforced concrete, Materials and Structures 26 (162) (1993) 486–494.
[23] B.L. Karihaloo, J. Wang, M. Grzybowski, Doubly periodic arrays of bridged cracks and short fibre-reinforced cementitious composites, Journal of the Mechanics and Physics of Solids 44 (10) (1996) 1565–1586.
[24] D. Lange-Kornbak, B.L. Karihaloo, Tension softening of fibre-reinforced cementitious composites, Cement and Concrete Composites 19 (4) (1997) 315–328.
[25] X.H. Guo, F. Tin-Loi, H. Li, Determination of quasibrittle fracture law for cohesive crack models, Cement and Concrete Research 29 (7) (1999) 1055–1059.
[26] M.T. Kazemi, F. Fazileh, M.A. Ebrahiminezhad, Cohesive crack model and fracture energy of steel-fiber-reinforced-concrete notched cylindrical specimens, Journal of Materials in Civil Engineering — ASCE 19 (10) (2007) 884–890.
[27] J.L.A. de Oliveira e Sousa, R. Gettu, Determining the tensile stress–crack opening curve of concrete by inverse analysis, Journal of Engineering Mechanics — ASCE 132 (2) (2006) 141–148.
[28] V. Slowik, B. Villmann, N. Bretschneider, T. Villmann, Computational aspects of inverse analyses for determining softening curves of concrete, Computer Methods in Applied Mechanics and Engineering 195 (52) (2006) 7223–7236.
[29] M. Elices, G.V. Guinea, J. Gomez, J. Planas, The cohesive zone model: advantages, limitations and challenges, Engineering Fracture Mechanics 69 (2) (2002) 137–163.
[30] J. Zhang, V.C. Li, Simulation of crack propagation in fiber-reinforced concrete by fracture mechanics, Cement and Concrete Research 34 (2) (2004) 333–339.
[31] J. Zhang, H. Stang, Applications of stress crack width relationship in predicting the flexural behavior of fibre-reinforced concrete, Cement and Concrete Research 28 (3) (1998) 439–452.
[32] J.E. Bolander, N. Sukumar, Irregular lattice model for quasistatic crack propagation, Physical Review B 71 (9) (2005) 94106-1–94106-12.
[33] A.R. Ingraffea, W.H. Gerstle, P. Gergely, V. Saouma, Fracture mechanics of bond in reinforced concrete, Journal of Structural Engineering 110 (4) (1984) 871–890.
[34] X.P. Xu, A. Needleman, Numerical simulations of fast crack growth in brittle solids, Journal of the Mechanics and Physics of Solids 42 (9) (1994) 1397–1434.
[35] G. Ruiz, M. Ortiz, A. Pandolfi, Three-dimensional finite-element simulation of the dynamic Brazilian tests on concrete cylinders, International Journal for Numerical Methods in Engineering 48 (7) (2000) 963–994.
[36] J. Roesler, G.H. Paulino, K. Park, C. Gaedicke, Concrete fracture prediction using bilinear softening, Cement & Concrete Composites 29 (4) (2007) 300–312.
[37] S.H. Song, G.H. Paulino, W.G. Buttlar, Simulation of crack propagation in asphalt concrete using an intrinsic cohesive zone model, Journal of Engineering Mechanics — ASCE 132 (11) (2006) 1215–1223.
[38] Z. Zhang, G.H. Paulino, Cohesive zone modeling of dynamic failure in homogeneous and functionally graded materials, International Journal of Plasticity 21 (6) (2005) 1195–1254.
[39] R. de Borst, M.A. Gutierrez, G.N. Wells, J.J.C. Remmers, H. Askes, Cohesive-zone models, higher-order continuum theories and reliability methods for computational failure analysis, International Journal for Numerical Methods in Engineering 60 (1) (2004) 289–315.
[40] Q. Xiao, B.L. Karihaloo, Asymptotic fields at frictionless and frictional cohesive crack tips in quasibrittle materials, Journal of Mechanics of Materials and Structures 1 (5) (2006) 881–910.
[41] Q.Z. Xiao, B.L. Karihaloo, X.Y. Liu, Incremental-secant modulus iteration scheme and stress recovery for simulating cracking process in quasi-brittle materials using XFEM, International Journal for Numerical Methods in Engineering 69 (12) (2007) 2606–2635.
[42] B.L. Karihaloo, Q.Z. Xiao, Asymptotic fields at the tip of a cohesive crack, International Journal of Fracture 150 (1–2) (2008) 55–74.
[43] J. Roesler, G. Paulino, C. Gaedicke, A. Bordelon, K. Park, Fracture behavior of functionally graded concrete materials for rigid pavements, Transportation Research Record 2037 (2007) 40–49.
[44] V. Ramakrishnan, S. Gollapudi, R. Zellers, Performance characteristics and fatigue strength of polypropylene fibre reinforced concrete, Fibre Reinforced Concrete Properties & Applications, SP-105, American Concrete Institute, 1987, pp. 141–158.
[45] Z. Bayasi, J. Zeng, Properties of polypropylene fiber reinforced concrete, ACI Materials Journal 90 (6) (1993) 605–610.
[46] J.G.M. van Mier, Fracture Processes of Concrete: Assessment of Material Parameters for Fracture Models, CRC Press, Boca Raton, 1996.
[47] K. Park, G.H. Paulino, J.R. Roesler, Determination of the kink point in the bilinear softening model for concrete, Engineering Fracture Mechanics 75 (13) (2008) 3806–3818.
[48] A. Hillerborg, The theoretical basis of a method to determine the fracture energy G_F of concrete, Materials and Structures 18 (4) (1985) 291–296.
[49] Z.P. Bazant, M.T. Kazemi, Determination of fracture energy, process zone length and brittleness number from size effect, with application to rock and concrete, International Journal of Fracture 44 (2) (1990) 111–131.
[50] Z.P. Bazant, Q. Yu, G. Zi, Choice of standard fracture test for concrete and its statistical evaluation, International Journal of Fracture 118 (4) (2002) 303–337.
[51] Y.S. Jenq, S.P. Shah, Two parameter fracture model for concrete, Journal of Engineering Mechanics — ASCE 111 (10) (1985) 1227–1241.
[52] C. Rocco, G.V. Guinea, J. Planas, M. Elices, Review of the splitting-test standards from a fracture mechanics point of view, Cement and Concrete Research 31 (1) (2001) 73–82.
[53] S.P. Shah, S.E. Swartz, C. Ouyang, Fracture Mechanics of Concrete: Applications of Fracture Mechanics to Concrete, Rock and Other Quasi-Brittle Materials, Wiley-Interscience, New York, 1995.
[54] T.L. Anderson, Fracture Mechanics: Fundamentals and Applications, CRC Press, Boca Raton, 1995.
[55] A.A. Griffith, The phenomena of rupture and flow in solids, Philosophical Transactions. Royal Society of London 221 (1920) 163–198.
[56] Standard Test Method for Flexural Toughness and First-Crack Strength of Fiber-Reinforced Concrete (Using Beam With Third-Point Loading), ASTM International, West Conshohocken, PA, 1997.
[57] Standard Test Method for Flexural Performance of Fiber-Reinforced Concrete (Using Beam With Third-Point Loading), ASTM International, West Conshohocken, PA, 2007.
[58] T.-S. Lok, J.-S. Pei, Flexural behavior of steel fiber reinforced concrete, Journal of Materials in Civil Engineering — ASCE 10 (2) (1998) 86–97.
[59] S.-Y. Fu, B. Lauke, Effects of fiber length and fiber orientation distributions on the tensile strength of short-fiber-reinforced polymers, Composites Science and Technology 56 (10) (1996) 1179–1190.
[60] V.S. Gopalaratnam, S.P. Shah, Tensile failure of steel fiber-reinforced mortar, Journal of Engineering Mechanics — ASCE 113 (5) (1987) 635–652.
[61] E.C.N. Silva, R.C. Carbonari, G.H. Paulino, On graded elements for multiphysics applications, Smart Materials and Structures 16 (6) (2007) 2408–2428.
[62] J.H. Kim, G.H. Paulino, Isoparametric graded finite elements for nonhomogeneous isotropic and orthotropic materials, Journal of Applied Mechanics — Transactions of the ASME 69 (4) (2002) 502–514.
[63] G.H. Paulino, J.-H. Kim, The weak patch test for nonhomogeneous materials modeled with graded finite elements, Journal of the Brazilian Society of Mechanical Sciences and Engineering 29 (1) (2007) 63–81.